

This work was written as part of one of the author's official duties as an Employee of the United States Government and is therefore a work of the United States Government. In accordance with 17 U.S.C. 105, no copyright protection is available for such works under U.S. Law.

Public Domain Mark 1.0













<https://creativecommons.org/publicdomain/mark/1.0/>

Access to this work was provided by the University of Maryland, Baltimore County (UMBC) ScholarWorks@UMBC digital repository on the Maryland Shared Open Access (MD-SOAR) platform.

**Please provide feedback**

Please support the ScholarWorks@UMBC repository by emailing [scholarworks-group@umbc.edu](mailto:scholarworks-group@umbc.edu) and telling us what having access to this work means to you and why it's important to you. Thank you.

# Effect of Space Radiation on Transition-Edge Sensor Detectors Performance

S. Beaumont , J.-M. Lauenstein , J. S. Adams, S. R. Bandler, J. A. Chervenak , F. M. Finkbeiner , S. V. Hull ,  
R. L. Kelley, C. A. Kilbourne , A. Le Roch, H. Muramatsu , F. S. Porter , K. Sakai , S. J. Smith ,  
N. A. Wakeham , E. J. Wassell , and S. Yoon

**Abstract**—The Athena mission and its X-ray Integral Field Unit (X-IFU) instrument will be positioned at the Sun-Earth Lagrange point L1, where it will be subject to particles from the solar wind with energy below 0.1 MeV, and from galactic cosmic rays and solar flares with energies up to hundreds of MeV for protons and GeVs for heavier ions. Some of these particles will go through the satellite and hit the focal plane assembly and hence the detectors. These detectors will be TES (Transition-edge sensor) microcalorimeters, flown for the first time in such an environment. In order to ensure the performance of this type of detector throughout the duration of such a mission, it is critical to study the impact of the radiation on their behavior. Indeed, although a lot of reference material exist for semiconductor-based photodetectors such as CCDs and CISs, little is currently known about the impact of radiation on TES detectors. These energetic events could cause local heating or damage to the detectors and affect their performance. In this work, we describe how we designed a test campaign to assess the impact of L1 radiation on TES detectors for Athena/X-IFU-like missions and present the results of the tests, for a maximum dose of 4.3 krad(Si). Analysis includes assessing changes in the pulse shapes and energy resolution of the detectors measured at 55 mK after several radiation dose steps performed at 4 K.

**Index Terms**—TES microcalorimeters, long term performance, radiation effects, permanent damage, total dose, displacement damage.

Manuscript received 18 November 2022; revised 1 March 2023; accepted 7 March 2023. Date of publication 7 April 2023; date of current version 2 May 2023. This work was supported in part by NASA under Grant 80GSFC21M0002 and in part by an appointment to the NASA Postdoctoral Program at the NASA Goddard Space Flight Center, administered by Oak Ridge Associated Universities under Contract with NASA. (*Corresponding author: S. Beaumont.*)

S. Beaumont, J. S. Adams, K. Sakai, and N. A. Wakeham are with the NASA Goddard Space Flight Center, Greenbelt, MD 20771 USA, and also with the University of Maryland Baltimore County, Baltimore, MD 21250 USA (e-mail: sbeaumont@umbc.edu).

J.-M. Lauenstein, S. R. Bandler, J. A. Chervenak, R. L. Kelley, C. A. Kilbourne, F. S. Porter, S. J. Smith, and E. J. Wassell are with the NASA Goddard Space Flight Center, Greenbelt, MD 20771 USA.

F. M. Finkbeiner and S. Yoon are with the NASA Goddard Space Flight Center, Greenbelt, MD 20771 USA, and also with the Sigma Space Corp, Lanham, MD 20706 USA.

S. V. Hull and A. Le Roch are with the NASA Goddard Space Flight Center, Greenbelt, MD 20771 USA, and also with the NASA Postdoctoral Program Fellows, Greenbelt, MD 20771 USA.

H. Muramatsu is with the NASA Goddard Space Flight Center, Greenbelt, MD 20771 USA, and also with the Catholic University of America, Washington, DC 20064 USA.

Color versions of one or more figures in this article are available at <https://doi.org/10.1109/TASC.2023.3264955>.

Digital Object Identifier 10.1109/TASC.2023.3264955

## I. INTRODUCTION

TRANSITION-EDGE sensor (TES) detectors which are being developed for astrophysical X-ray observations will hence be operated in space for several years, where they will face the potentially damaging space environment. This is for instance the case for the X-ray Integral Field Unit (X-IFU) instrument [1], onboard the Athena (Advanced Telescope for High Energy Astrophysics) mission, scheduled for launch in the 2030's, for a mission duration of 4 years (with a possible extension to 10 years) at the Sun-Earth Lagrange point L1. At such orbit, it will be subject to cosmic rays (CRs) with energies less than 0.1 MeV all the way to the GeV per nucleon range. The low energy particles come mainly from the solar wind made of a low flux of protons (95%) and alpha particles (5%), and the energetic particles from galactic cosmic rays (GCRs) and coronal mass ejections, made of protons, alphas, and electrons with energies up to hundreds of MeV for H+ and the GeV per nucleon for heavier ions.

A lot of literature and data related to the impact of space radiation exists on semiconductor-based detectors such as CCDs or CISs [2] which have been used in space instruments for many years and extensively studied, showing obvious impact of space radiation on their behavior. Several studies can also be found regarding superconductors [3] or Josephson junctions [4], [5], [6]. TESs however, at the exception of sounding rockets [7], have not been flown yet and little studies exist. It is hence crucial to understand whether space radiation may impact their performance over the mission duration.

Several potential radiation-induced vulnerabilities in TESs were suggested prior to performing measurements. Radiation effects can generally be split into two main categories: cumulative dose and single event (or transient) effects. In this paper, we focused on potential permanent cumulative damage, which can themselves be separated between Total Non-Ionizing dose (TNID) and Total ionizing dose (TID) damage. Although there is usually no performance degradations related to atomic displacements in metals unless the level of radiation is very high, displacements impacts on superconductors operating at cryogenic temperature where the atoms cannot move around to heal had to be considered. Displacements could for instance impact the normal state resistance and/or the critical current in the TES bilayer, or in the leads creating magnetic flux trapping issues. Displacement damage could also affect the absorbers, with concerns on how subtle changes could potentially lead to large impacts in properties, affecting the pulse shape (secondary time constants, rise time, amplitude) and/or the energy spectrum (excess broadening, low energy tail). Dislocations in the oxide

layers however were expected to have no measurable effects due to the amorphous structure of the oxide. In terms of ionizing dose, charge trapping in the bulk oxide layers could occur but were not considered as a high risk given the low biases involved. Interface traps located at the oxide interfaces were also considered but expected to be low risks due to the charge trapping and de-trapping effect mechanisms being thermally activated and so unlikely for our low-temperature detectors.

In this work, we detail how we designed and implemented a radiation test campaign in order to assess the impact of radiation on TES detectors (see Section II) and present the corresponding results (see Section III).

## II. TEST DESIGN

### A. General Philosophy

TES detectors are superconducting devices which must be operated at cryogenic temperatures; it was therefore important to design the radiation tests accordingly. Indeed, dose effects are temperature dependent with no hard threshold above which annealing of damage or trapped charge begins. Typically, annealing occurs more rapidly with increasing temperature. It was hence particularly important to perform these tests at a low enough temperature to be representative of the level of impact from the expected on-orbit radiation and maintain a low enough temperature between dose steps to make sure no annealing happened. The flux necessary for an accelerated dose test would generate too much heat to be able to maintain the 55 mK TES operational temperature during irradiation. Thus, it was decided to deliver the radiation doses at 4 K, interleaved by characterization of the detectors at 55 mK. As little is known about proton radiation effects in such detectors, an additional TES detector chip was also irradiated at room temperature (295 K). Details about the test plan and how it was designed are given in the upcoming sections.

### B. Dose Levels and Beam Energy

1) *Radiation Transport Analysis*: To evaluate the dose received at the detector level, it is necessary to perform a radiation transport analysis based on the cosmic ray spectrum reaching the spacecraft and the various shields protecting the component (e.g., the satellite, the dewar, etc). Such analysis can be done using a full sectorial analysis, or Monte-Carlo approach. In this project, an adjoint Monte-Carlo shielding analysis was performed to determine mission-relevant total dose levels using the software NOVICE [8]. This was done using a simplified CAD model of the TES chip surrounded by concentric spherical shells of materials representing the satellite, cryostat, and focal plane assembly. The spherical representations were made following some work at the X-IFU level for the non-X-ray background studies [9]. The spacecraft shielding assumptions include 11.2 mm of aluminum, with two interleaving layers of MLI (multi-layer insulation). However, an additional transport analysis was performed using a 3 mm Al spacecraft layer instead of 11.2 mm, to ensure the test dose levels met worst-case shielding assumptions. In both cases, other instrument mass adds an additional 7.66 mm equivalent aluminum shielding due in part to a 0.5 mm Nb layer, 1 mm cryoperm (Fe) layer, and 2.65 mm Al outer layer.

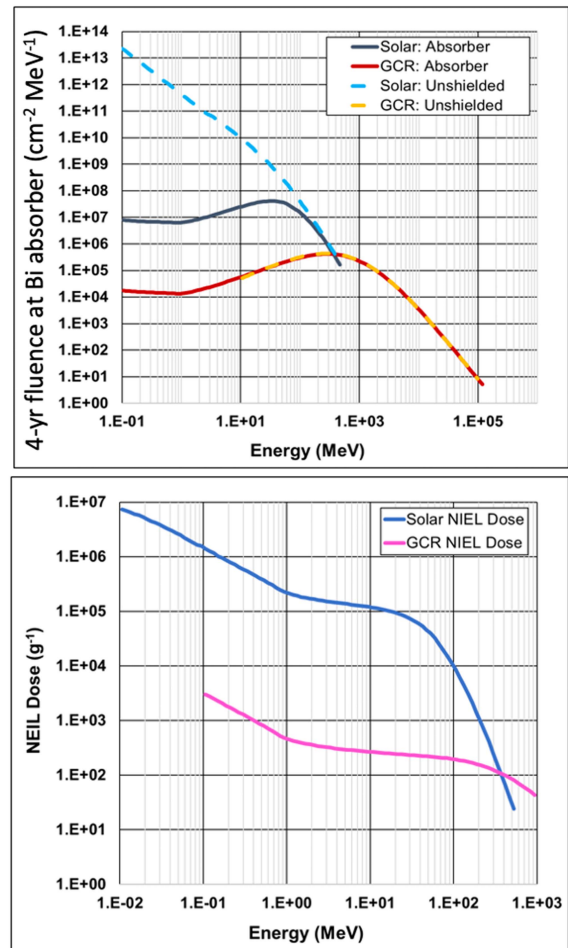


Fig. 1. (Top) 4-year shielded and unshielded fluence at the Bi absorber level. (Bottom) NEIL dose from the solar and GCR components.

For the input proton spectra at Lagrange point L1, for a 4-yr mission requirement lifetime and 10-yr mission extended lifetime, both CR components coming from the Sun and from other astrophysical sources were considered. The un-shielded solar proton fluence was determined using the ESP (Emission of Solar Protons) model [10] available on ESA's SPENVIS (SPace ENVironment Information System) platform [11]. The ESP model was run at 90% confidence level, for either 4 years at solar maximum or for 10 years of which 7 years were at solar maximum. To account for the orbit of the mission at less than 1 AU from the Sun, a  $1/r^2$  scaling factor with  $r = 0.99$  was applied. The galactic cosmic ray (GCR) component was obtained from the GCR proton flux specified in an X-IFU internal technical note written by INAF, and scaled up to match fluences for 4-yr and 10-yr mission durations.

Although outputs from NOVICE (i.e., total ionizing dose (TID) levels and transported proton energy spectra) were computed for several point locations on the TES chip, values used for designing the test were chosen where the dose levels were highest, i.e., at the center of the bismuth absorber. The initial un-shielded spectra, and the spectra at the TES chip bismuth absorber provided by NOVICE, are shown in Fig. 1.

To determine the expected total non-ionizing dose (TNID) for the detector chip, these spectra were weighted by the Coulombic

Mission duration	1 yr dose	2 yr dose	4 yr dose	10 yr dose	~25 yr dose
Exposure [min]	61.0	47.5	88.5	202.8	336.7
Fluence [ $\text{cm}^{-2}$ ]	1.78 e+9	3.56 e+9	7.12 e+9	1.32 e+10	3.26 e+10
TNID [ $\text{MeV/g(Bi)}$ ]	1.67 e+6	3.33 e+6	6.67 e+6	1.24 e+7	3.05 e+7
TID [ $\text{rad(Bi)}$ ]	139	278	557	1032	2548
TID [ $\text{rad(Si)}$ ]	234	467	934	1732	4282
System at :	4 K	*1 4 K	4 K	4 K	*2 4 K

TES characterization at 55 mK

Fig. 2. Table summarizing the dose steps delivered at 4 K to our TES detector. Given fluences, TNIDs and TIDs are cumulative values. \*1 and \*2 respectively mark warm up of the cryostat to room temperature and 20 K.

interaction portion of the non-ionizing energy loss (NIEL) for protons in bismuth, as determined by the SR-NIEL calculator [12]. The results are shown at the bottom of Fig. 1.

2) *Beam Energy*: Fig. 1 shows that most damage will occur from protons with energy less than 1 MeV. However, the SR-NIEL calculator does not include values for nuclear interactions in bismuth, therefore potentially underestimating the damage from higher energy protons. For this proton test campaign, an initial beam energy of 64 MeV was chosen for reduced energy straggle upon passage through the dewar windows, better uniformity of proton energy through the TES chip layers, and to produce larger damage clusters that may be more disruptive to superconductor properties. The initial 64.05 MeV proton beam resulted in a surface-incident energy of  $63.77 \pm 0.05$  MeV at the detector after passing through a 7 mil Be dewar window and three  $2 \mu\text{m}$  aluminized mylar layers.

3) *Proton Exposures*: 64 MeV proton beam exposures were conducted at high flux to deposit the total dose. At this energy, protons deposit more total ionizing dose in bismuth than non-ionizing dose. For this reason, fluence levels were determined by the TNID dose steps, and thus exceeding the expected TID level for the representative time on orbit.

As previously mentioned, the detector chip was maintained at 4 K during irradiation. Fig. 2 provides the beam run information, including cumulative TNID steps, equivalent proton fluence, and cumulative TID for bismuth. It should be noted that after the 1-yr dose the system had to be warmed to room temperature, and so annealing of the prior dose was assumed, with the next beam run therefore delivering a full 2-year dose. After the 4-yr dose, the system was warmed up to 20 K and cooled down again to 4 K in order to fix a trapped flux issue. Because the temperature did not exceed 20 K, it was assumed that no annealing had occurred.

The final dose step resulted in TNID and TID levels meeting or exceeding those expected for a 25-year mission when 11 mm aluminum equivalent spacecraft shielding is assumed. These levels also bounded a 10-yr mission dose based on the more conservative 3 mm Al equivalent spacecraft shielding.

For the warm irradiation, a second test chip was exposed at room temperature (295 K) to an equivalent proton fluence yielding a 20-year mission dose, i.e.,  $2.64 \times 10^{10} \text{ cm}^{-2}$ .

### C. Radiation Test Facility

The testing was conducted at the Crocker Nuclear Laboratory (CNL) at the University of California, Davis Campus (UC Davis). The facility utilizes a 76-inch variable-energy Isochronal cyclotron, which can provide tunable proton energies up to 67 MeV in air. The maximum beam spot is 3 cm in radius. In our case, a 1-inch diameter circular collimator was placed at

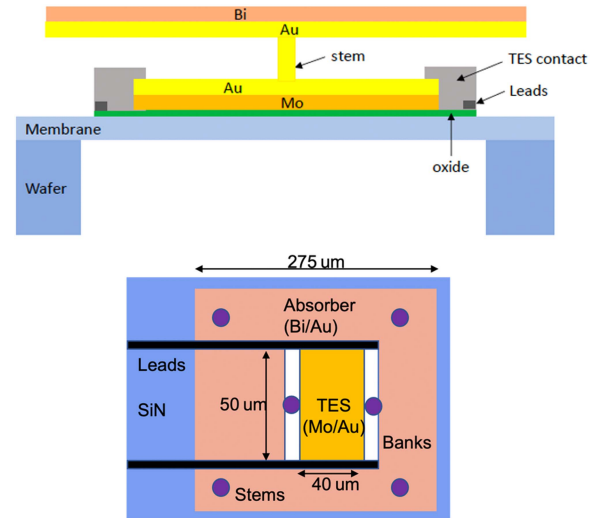


Fig. 3. (Top) Simplified representation of our TES detectors seen from the side. (Bottom) 2D view from the top, for one of the TES aspect ratios and number of dotted stems configuration.

the end of the beam line to reduce nuclear activation of materials surrounding the TES chip. A combination of secondary electron emission measurements and a retractable Faraday cup are used for dosimetry for proton flux at or greater than  $10^5 \text{ cm}^{-2} \text{ s}^{-1}$ . A table for mounting experiments is set-up in front of the beam port and allows for vertically and horizontally controlled motions. The alignment of the target is achieved with a pointer and with a laser beam.

### D. Test Setup

The complexity of the setup for this test campaign limited the number of samples which could be irradiated. One  $32 \times 32$  TES chip was installed as our primary sample for cold irradiation, while another  $8 \times 8$  TES chip was installed on a second available detector assembly fitting our cryostat, initially as back-up for the cold irradiation and in the end used for an additional warm irradiation of the detectors and characterization once back at NASA Goddard Space Flight Center (GSFC).

For both TES chips, the TES is made of a Mo/Au bilayer (respectively  $\sim 44$ – $47$  nm and  $\sim 240$ – $323$  nm thick) deposited on a  $0.5 \mu\text{m}$ -thick  $\text{Si}_x\text{N}_y$  membrane and  $300 \mu\text{m}$ -thick Si wafer. Two gold banks, parallel to the current flow, are deposited at the edge of the bilayer and on top of each of them are dotted stems used to attach the absorber. The absorbers consist of two square electroplated layers of Au and Bi with respective thicknesses of  $3.1$  and  $1.3 \mu\text{m}$ , with  $275 \mu\text{m}$  side length. They are supported by 2 or 4 additional stems going to membrane, as shown on Fig. 3. On the small TES chip, an additional  $40$  nm thick Au capping layer was included. Different TES designs were present on the chips and connected:  $50 \times 40 \mu\text{m}$  (TES length  $\times$  width) with either 4 or 6 dots on the  $32 \times 32$  TES chip, and additional  $50 \times 50 \mu\text{m}$  with 6 dots and  $60 \times 30 \mu\text{m}$  with 4 or 6 dots on the  $8 \times 8$  TES chip. The microstrip bias lines were composed of  $\sim 160$  nm of Nb,  $\sim 250$  nm of  $\text{SiO}_2$ , and  $\sim 240$  nm of Nb. Finally, there was a thin oxide layer, remnant from the fabrication process, of  $\sim 155$  nm between the TES and the membrane.

Those TES chips were installed on a 55 mK detector assembly, housing as well Nyquist and MUX SQUID chips provided by



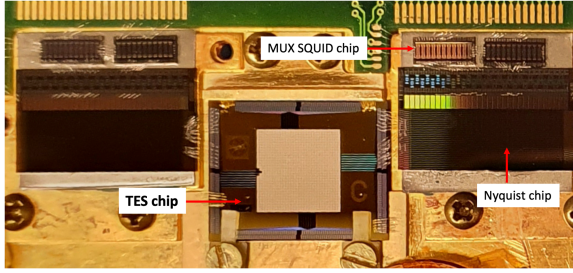


Fig. 4. Picture of the  $32 \times 32$  TES chip used for the cold irradiation test, installed on the 55 mK detector assembly, and wirebonded to the Nyquist and MUX SQUID chips.

NIST [13], as shown on Fig. 4. The rest of the readout chain was composed of AMP SQUIDS at the 4 K stage and a Warm Front-End Electronics both provided by NIST, as well as a Digital Readout Electronics developed inhouse from GSFC [14]. This provided a single channel readout system for 2 columns, where up to 26 pixels could be connected (13 on each of the 2 quadrants of the TES chip).

However, based on the available time for characterization between each dose step and the lack of proper multiplexed readout on that system, only a subset of pixels could be looked at: transition shapes for 4 pixels per run, pulse shapes for 16 pixels per run, and noise and X-ray spectra for up to 4 pixels per run.

X-rays are provided by 2 different sources: an Fe-55 electron capture source, producing X-rays at 5.9 keV (Mn-K $\alpha$ ), and portable channel-cut crystal monochromator (CCCMs) built at GSFC [15] producing X-rays at 5.4 keV.

### III. RESULTS AND DISCUSSION

#### A. Cold Irradiation

1) *Impact on Transition Shapes:* The analysis of the transition shapes showed they were very stable over the different irradiation steps. No apparent sign of critical temperature ( $T_c$ ) shift due to radiation was observed. Some small differences (less than 3%) from the data taken the first day at CNL can be seen but are attributable to changes in the ambient conditions (such as a slightly different magnetic field environment). An example of transition shapes after each step for 2 different pixels is provided on Fig. 5.

2) *Impact on Pulse Shapes:* The X-ray pulse shapes also appear to be stable over the different irradiation steps, as shown in Fig. 6 for two of the tested pixels, before and after the various dose steps. A somewhat larger difference after the 2- and 4-year doses can be observed; however, data (including the response of the SQUID readout to feedback current) suggested the presence of magnetic field trapping inside the Nb box after the system had to be warmed up to room temperature and cooled down again between the 1-year and 2-year doses. This difference was reduced back to a level close to zero after the system was partially warmed up (to 20 K) after the 4-year dose.

The pulse shapes, which present a secondary time constant from the start (from the thermal heating of the substrate from X-rays, and the corresponding heat flowing away on a slightly slower time constant [16]), did not present visible change in height or in the secondary tail due to irradiations. As for the transition shapes, the small differences which can be observed

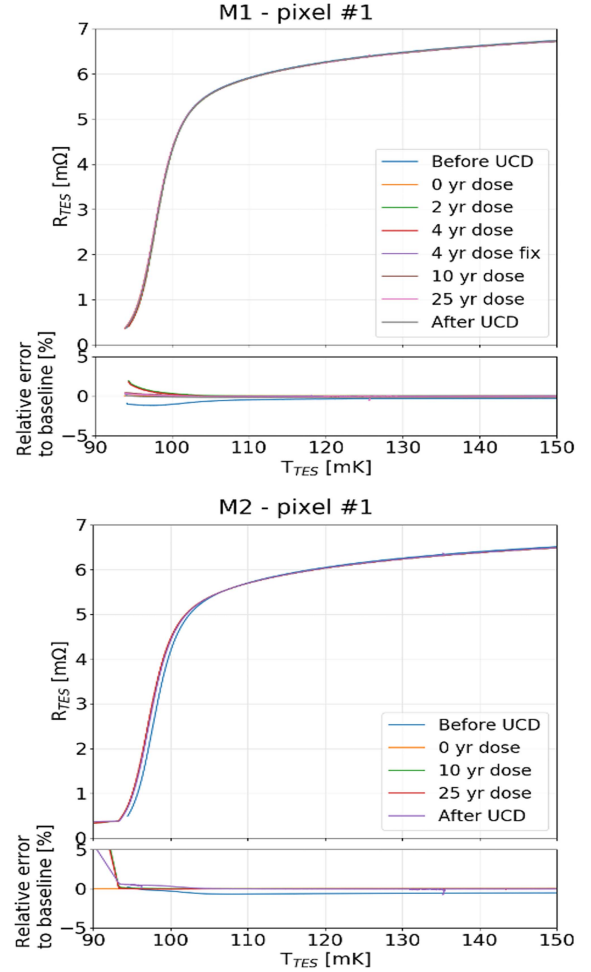


Fig. 5. Transition shapes for 2 different pixels before and after each step of the proton irradiation. Those show little to no variation after the various dose.

can be attributed to changes in ambient conditions (slightly different field environment, bias points).

3) *Impact on Energy Resolution:* The energy resolution from  $^{55}\text{Fe}$  and with the monochromatic source, as determined by full width at half maximum amplitude (FWHM), appears to be fairly stable over the different radiation steps as shown for one of the tested pixels (Fig. 7). Although not shown here, there is also no sign of low energy tail appearing on the data taken with the mono source [15].

One point with a degradation in energy resolution can be observed after the 25-year dose, but which can be correlated with higher low-frequency noise as shown on Fig. 8. This appeared to be due to higher background noise coming from the Nb box. Gamma rays were produced by the activated niobium, hitting the detector, and affecting the temperature stability and noise level, leading to a degraded resolution as well as NEP. Also, once re-measured after a several hours the noise level at low frequencies had started to lower back down.

The last data point in Fig. 7 corresponds to data measured at GSFC upon return from UC Davis, i.e., after the system had warmed up and annealing could happen over about 2 weeks. It is hence not a directly representative data point in terms of robustness to radiation while in space but was interesting to show that the system had returned to its original performance.

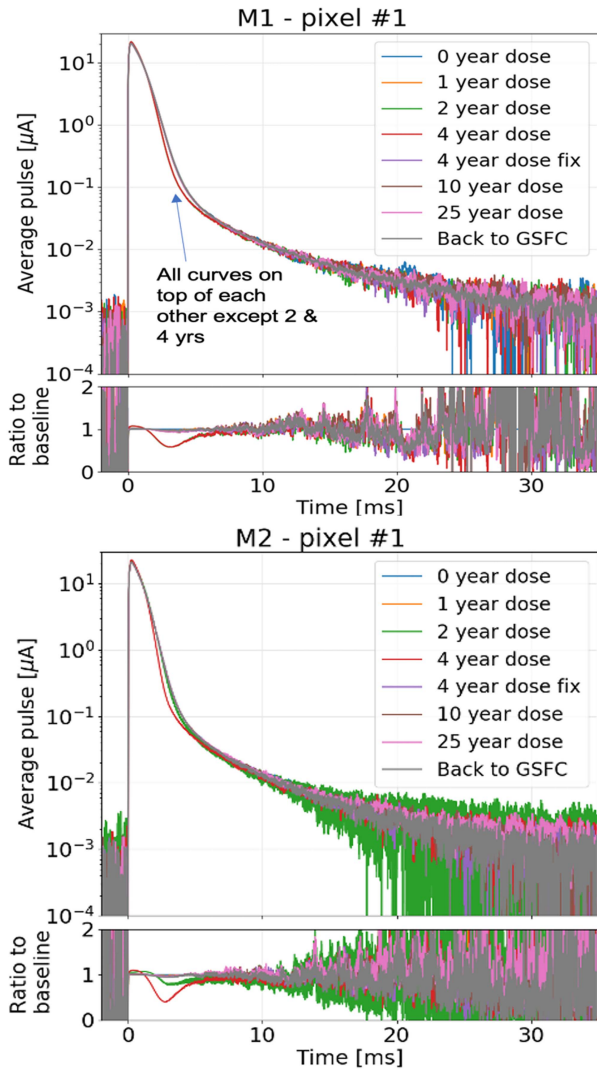


Fig. 6. Pulse shapes for 2 different pixels before and after each step of the proton irradiation. Those show little to no variation after the various dose, except after the 2- and 4- year dose where trapped flux was present.

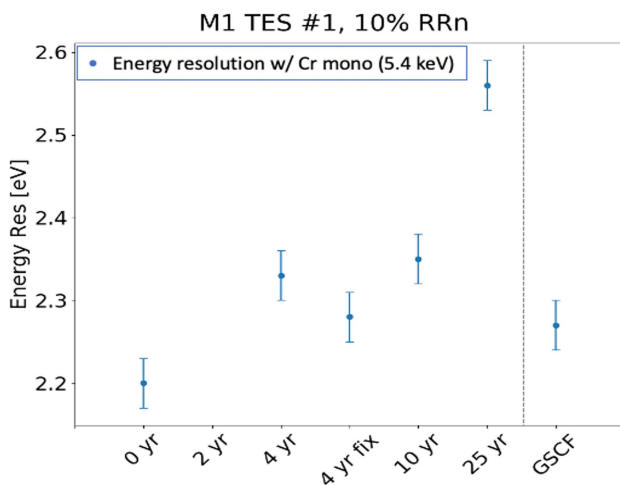


Fig. 7. Energy resolution measured with the Cr-CCCM X-ray source for one of the measured pixels, plotted as a function of the dose step. The last point corresponds to data measured after the system had been warmed up and shipped back to GSFC.

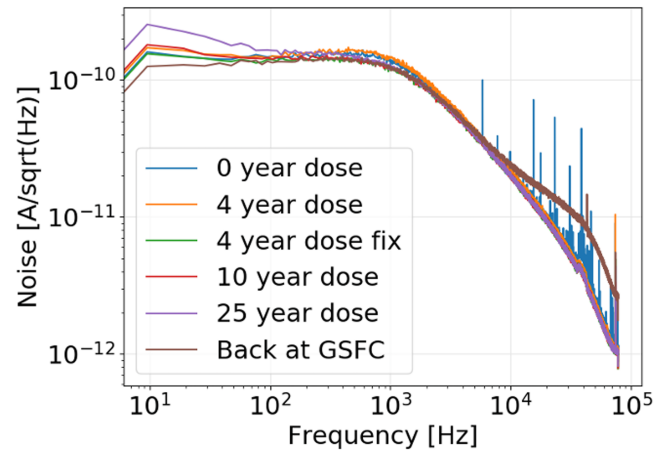


Fig. 8. Noise spectra for one of the measured pixel, after different radiation dose steps. Those show a clear increase in low frequency after the 25 year dose step.

### B. Warm Irradiation

For the warm irradiation test, the TES chip was placed inside the cryostat and characterized at 55 mK after returning to GSFC. The transition shapes, pulse shapes, and energy resolution were compared before and after irradiation, and consistent with the cold irradiation showed no evidence of changes due to the delivered radiation dose.

An example of pulse shape overlay before and after irradiation is shown in Fig. 9, with a slightly different offset field applied. Some small differences were again, as after the cold irradiation, visible in the transition and pulse shapes, but likely due to changes in the environment which can induce run-to-run variations as illustrated by the data with different offset fields.

## IV. CONCLUSION

We designed and performed a radiation test campaign to assess the robustness to space radiation of TES detectors such as those being developed for the Athena/X-IFU instrument. Due to the complexity of performing such experiment while at low temperature, this had not been done before, and provides new information regarding permanent damage (or rather the lack of damage) to TES sensors.

From both the cold and warm irradiation tests, results show no clear degradation in the TESs performance for a maximum dose from  $3.26 \times 10^{10} \text{ cm}^{-2}$  64-MeV proton fluence (or 2.5 krad(Bi), equivalent to 4.3 krad(Si)), equivalent to a mission duration of  $\sim 25$  years based on 11.2 mm aluminum spacecraft and  $\sim 7.7$  mm equivalent Al instrument shielding. This is also equivalent to a 10-year mission duration with 3 mm aluminum spacecraft shielding plus additional instrument layers.

More specifically, no performance degradation was observed in the transition shapes, the pulse shape, or the energy resolution performance and spectral redistribution. Some minor variations were observed but are within the range of the typical run-to-run variability of pulse shapes/heights and R vs T variation, which can be explained by small variations in the environment (such as magnetic field or bias point).

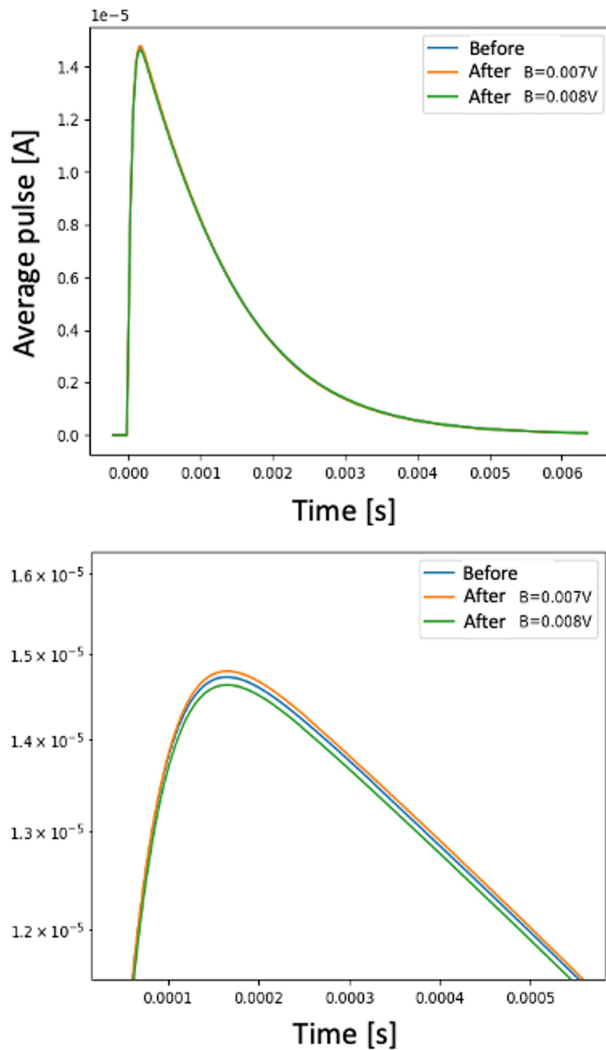


Fig. 9. Pulse shape for one of the tested pixels before and after the warm irradiation. A small change in pulse height can be observed, although attributed to slightly different local field conditions between both cool-downs.

Those tests hence successfully addressed the risk associated with the TES detectors being robust to the space environment at L1 for a mission duration of 10 years.

## REFERENCES

- [1] D. Barret et al., "The athena X-ray integral field unit (X-IFU)," *Proc. SPIE Space Telescopes Instrum.: Ultraviolet to Gamma Ray*, vol. 9905, 2016, Art. no. 99052F.
- [2] J. Janesick, J. T. Andrews, and T. Elliott, "Fundamental performance difference between CMOS and CDD imagers," *Proc. SPIE Space Telescopes Instrum.*, vol. 6276, 2006, Art. no. 62760M.
- [3] A. R. Sweedler, D. E. Cox, and S. Moehlecke, "Neutron irradiation of superconducting compounds," *J. Nucl. Mater.*, vol. 72, no. 1/2, pp. 50–69, 1978.
- [4] S. E. King, R. Magno, and W. G. Maisch, "Radiation damage assessment of Nb tunnel junction devices," *IEEE Trans. Nucl. Sci.*, vol. 38, no. 6, pp. 1359–1364, Dec. 1991.
- [5] M. Ohkubo, I. Sakamoto, T. Miura, and N. Hayashi, "Radiation effects in superconducting-tunnel-junction X-ray detectors," *Nucl. Instrum. Methods Phys. Res. Sect. A: Accelerators, Spectrometers, Detectors Assoc. Equip.*, vol. 399, no. 2/3, pp. 343–346, 1997.
- [6] S. Pagano et al., "Effect of intense proton irradiation on properties of Josephson devices," *IEEE Trans. Appl. Supercond.*, vol. 7, no. 2, pp. 2917–2920, Jun. 1997.
- [7] A. J. F. Hubbard et al., "Design and status of the micro-X microcalorimeter sounding rocket," *J. Phys.: Conf. Ser.*, vol. 1342, 2020, Art. no. 012096.
- [8] T. M. Jordan, "An adjoint charged particle transport method," *IEEE Trans. Nucl. Sci.*, vol. 23, no. 6, pp. 1857–1861, Dec. 1976.
- [9] S. Lotti et al., "Updates on the background estimates for the X-IFU instrument onboard of the ATHENA mission," *Proc. SPIE Space Telescopes Instrum.: Ultraviolet to Gamma Ray*, vol. 9905, 2016, Art. no. 990563.
- [10] M. A. Xapsos, G. P. Summers, J. L. Barth, E. G. Stassinopoulos, and E. A. Burke, "Probability model for cumulative solar proton event fluences," *IEEE Trans. Nucl. Sci.*, vol. 47, no. 3, pp. 486–490, Jun. 2000.
- [11] D. Heynderickx, B. Quaghebeur, and H. D. R. Evans, "The ESA space environment information system (SPENVIS)," in *Proc. IAF Abstr. 34th COSPAR Sci. Assem.*, 2002, Art. no. 475.
- [12] M. J. Boschini, P. G. Rancoita, and M. Tacconi, "SR-NIEL calculator: Screened relativistic (SR) treatment for calculating the displacement damage and nuclear stopping powers for electrons, protons, light- and heavy-ions in materials," version 7.7.3, INFN sez, Milano-Bicocca, Italy, 2014. Accessed: Sep. 2022. [Online]. Available: <http://www.sr-niel.org/>
- [13] M. Durkin et al., "Demonstration of athena X-IFU compatible 40-row time-division-multiplexed readout," *IEEE Trans. Appl. Supercond.*, vol. 29, no. 5, Aug. 2019, Art. no. 2101005.
- [14] K. Sakai et al., "Developments of laboratory-based transition-edge sensor readout electronics using commercial-off-the-shelf modules," *J. Low Temp. Phys.*, vol. 209, pp. 743–749, 2022.
- [15] M. E. Eckart et al., "Extended line spread function of TES microcalorimeters with Au/Bi," *IEEE Trans. Appl. Supercond.*, vol. 29, no. 5, Aug. 2019, Art. no. 2101205.
- [16] A. R. Miniussi et al., "Thermal crosstalk measurements and simulations for an X-ray microcalorimeter array," *J. Low Temp. Phys.*, vol. 199, pp. 663–671, 2020.